Chemosphere 271 (2021) 129522

Contents lists available at ScienceDirect

Chemosphere

journal homepage: www.elsevier.com/locate/chemosphere

Application of aerobic kenaf granules for biological nutrient removal in a full-scale continuous flow activated sludge system

Stephany P. Wei [a, *], Bao Nguyen Quoc [a], Madelyn Shapiro [a], Pin Hsuan Chang [b], Jason Calhoun [b], Mari K.H. Winkler [a]

[a] University of Washington, Department of Civil & Environmental Engineering, 616 Northlake Place, Seattle, WA, 98195, USA
[b] Nuvoda, 608 Gaston Street Raleigh, NC, 27603, USA

HIGHLIGHTS

- Full-scale integration of aerobic kenaf granules in continuous flow system.
- SVI_{30} reduction from >200 to 50 mL g^{-1}.
- Increased EBPR efficiency with 25% dosage reduction for chemical P removal.
- Physical characteristics of kenaf granules met standards of aerobic granular sludge.
- Specific ammonia and phosphorus removal rates comparable to aerobic granules.

GRAPHICAL ABSTRACT

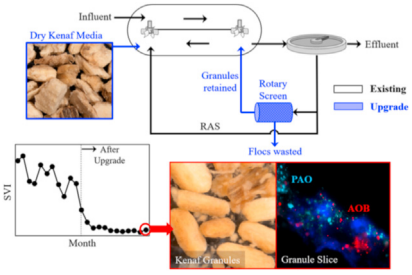

ARTICLE INFO

Article history:
Received 23 August 2020
Received in revised form
28 December 2020
Accepted 29 December 2020
Available online 31 December 2020

Handling Editor: Hyunook Kim

Keywords:
Aerobic granular sludge
EBPR
Continuous flow
Kenaf

ABSTRACT

Aerobic granular sludge (AGS) is a biofilm technology that offers more treatment capacity in comparison to activated sludge. The integration of AGS into existing continuous-flow activated sludge systems is of great interest as process intensification can be achieved without the use of plastic-based biofilm carriers. Such integration should allow good separation of granules/flocs and ideally with minor retrofitting, making it an ongoing challenge. This study utilized an all-organic media carrier made of porous kenaf plant stalks with high surface areas to facilitate biofilm attachment and granule development. A 5-stage Bardenpho plant was upgraded with the addition of kenaf media and a rotary drum screen to retain the larger particles from the secondary clarifier underflow whereas flocs were selectively wasted. Startup took 5 months with a sludge volume index (SVI) reduction from >200 to 50 mL g^{-1}. Most of the kenaf granules fell in the size range of 600–1400 μm and had a clear biofilm layer. The wet biomass density, SVI_{30}, and SVI_{30}/SVI_5 of the kenaf granules were 1035 g L^{-1}, 30.6 mL g^{-1}, and 1.0, respectively, which met the standards of aerobic granules. Improved stability of biological phosphorus removal performance enabled a 25% reduction in sodium aluminate usage. Microbial activities of kenaf granules were compared with aerobic granules, showing comparable N and P removal rates and presence of ammonium-oxidizing bacteria and polyphosphate-accumulating organisms in the outer 50–60 μm layer of the granule. This work is the first viable example for integrating fully organic biofilm particles in existing continuous-flow systems.

* Corresponding author. 616 Northlake Place, Seattle, WA, 98195, USA.
E-mail addresses: spw6422@uw.edu (S.P. Wei), quocbao@uw.edu (B. Nguyen Quoc), madelyn424@gmail.com (M. Shapiro), sage@nuvodaus.com (P.H. Chang), jason@nuvodaus.com (J. Calhoun), mwinkler@uw.edu (M.K.H. Winkler).

https://doi.org/10.1016/j.chemosphere.2020.129522
0045-6535/

1. Introduction

With the growing world population, sustainable wastewater treatment and environmental preservation are faced with increasing challenges, such as the need for wastewater treatment plants (WWTP) to add treatment capacity while being limited in space and resources (Winkler and Straka, 2019). The use of biofilm technologies such as aerobic granular sludge (AGS) has been an effective way to intensify existing wastewater infrastructure. Aerobic granules are dense spherical biofilm aggregates with high thickening and fast settling characteristics, thus its application can result in significant reduction in footprint and energy demand (Pronk et al., 2015). In contrast to other attached-growth biofilm technologies, such as the integrated fixed film activated sludge process, aerobic granules are naturally occurring biofilms which do not grow on plastic carriers that need to be landfilled.

AGS systems have been well-demonstrated in sequencing batch reactors (SBR) and a critical limitation of an SBR-type AGS system is that it requires tall reactors to enable good separation of slow and fast settling particles. Such configuration is therefore not easily retrofittable into continuous flow activated sludge (CFAS) systems without major modifications and sometimes decommissioning of the existing plant. Many lab-scale studies have cultivated granules in continuous-flow reactors, but they mostly rely on some variations of complex settler design to incorporate fast washout as a selection pressure for granule growth (Kent et al., 2018), which is not convenient to implement in existing full-scale CFAS plants. The use of seeding material (e.g. crushed granules or granular activated carbon) has been shown to enhance the granulation process by acting as nucleation sites for bacterial attachment (Li et al., 2011; Pijuan et al., 2011), which could be applied in CFAS systems to facilitate granule growth. However, seeding with granules is not always feasible for full-scale application because aerobic granules can take a long time to cultivate and are generally not available in large quantities. An attractive alternative would be an organic carrier that does not rely on plastic material or need to be cultivated beforehand. Organic carriers provide similar benefits as plastic carriers (e.g., increased treatment capacity in existing infrastructure), but are organic and may therefore undergo anaerobic digestion for sludge stabilization and resource recovery whereas plastic carriers must be land-filled.

In a CFAS system with integrated granular sludge, flocs and granules coexist and compete for substrates. Therefore, the proposed strategies for facilitating and maintaining granule growth in a CFAS system is to provide selective feeding of organic substrate to the granules and control granular sludge at higher sludge retention time (SRT) than flocculent sludge. To achieve these selective advantages for the granules, the physical separation of granules and flocs is key and research is currently focusing on sieving, hydraulic separators, or hydrocyclones (Kent et al., 2018; Sturm et al., 2017). In this work, a lignocellulosic carrier media made from kenaf plant (kenaf media) was seeded into a full-scale CFAS WWTP to facilitate biofilm attachment. Along with flocs, the kenaf media flow freely to the secondary clarifier, from which the underflow was separated into flocculent and kenaf particulate sludge with a rotary drum screen. Kenaf particles were then recycled back to the oxidation ditch and retained in the system while flocs were wasted.

The objectives of this study were to (1) explore the feasibility of the integration of granular sludge technology at an existing full-scale CFAS plant by seeding organic kenaf based carriers and retaining large particles, (2) discuss the improvements in settling and biological nutrient removal capacities, and (3) compare the developed kenaf biofilm particulates with aerobic granules in terms of physical characteristics and activities of key microbial functional groups.

2. Methods

2.1. Plant description and upgrade

The Town of Moorfield Advanced Nutrient WWTP (WV, USA) (Plant) is a 15.5 MLD 5-stage Bardenpho plant treating roughly 10% municipal wastewater and 90% industrial wastewater from a local poultry manufacturing facility. The averaged influent data are shown in Table S1 and the time series concentrations and loading are provided in Fig. S1 and Fig. S2, respectively. The Plant was upgraded with the Nuvoda's Mobile Organic Biofilm (MOB™) process, which involved the addition of organic media carriers made of kenafs to the oxidation ditch. To aid the adaptation of the MOB™ process, other plant-specific upgrades were made, including a 68 m^3 h^{-1} rotary drum screen (mesh size 500 μm), a 3.8 m^3 waste activated sludge (WAS) holding tank, and a belt filter press dewatering system (Fig. 1). Upon completion of the construction (March 9th, 2017), a single seeding event of about 50,325 kg of kenaf media was added directly to the oxidation ditch for a target fill ratio of 0.0033 kg of media per L of reactor volume. Flow from the oxidation ditch exited via a weir and moved to the center well of the secondary clarifiers. After the secondary clarifier underflow, a rotary drum screen was installed within the existing WAS line, which received on average 2.08 ML per week of flow. The cake (kenaf particles) from the rotary screen was returned to the reaeration zone of the ditch by gravity while the filtrate (flocs) was directed to sludge handling. As a result, only flocculent sludge was wasted from the system whereas kenaf particles were retained to ensure sufficient retention time for bacterial attachment and biofilm development on the kenaf particles. The dissolved oxygen (DO) setpoint in the aerobic zone was 0.35–0.5 mg L^{-1}. Sodium aluminate was dosed at a constant speed at the primary clarifier for chemical phosphorus removal, and the feed was manually increased whenever effluent TP raised above 0.7–0.8 mg L^{-1} for a few days. Supplemental carbon (glycerin) was added in the post-anoxic zone based on a nitrate sensor (Hach Nitratax sc) to maintain a nitrate level below 3.5 mg L^{-1}.

The kenaf media was made of renewable lignocellulosic material harvested from the kenaf plant, *Hibiscus cannabinus*, which was grown and processed at a local farm in Cameron, NC (USA). The kenaf media is approximately 1 mm in size with an estimated outer specific surface area (SSA) of greater than 20,000 m^2 $(m^3)^{-1}$ and total SSA greater than 463,000 m^2 $(m^3)^{-1}$ (Fig. S3a). Kenaf is a fast-growing plant with high adaptation to wide range of climate conditions (Ramesh, 2016). Like other natural plant fibers, it is considered a renewable material due to its high crop yield, minimal energy requirements, and biodegradability (Akil et al., 2011).

2.2. Plant data and sample collection

Twenty-four months of process data (twelve months each before and after the upgrade) was collected from the plant, which included 3 or 4 measurements per week of influent and effluent flows, BOD, TP, and NH_4^+, as well as effluent TN, NO_2^-, and NO_3^-. Weekly MLSS and monthly SVI_{30} were determined from grab samples collected from the oxidation ditch at about 4 ft from the surface (1/4 of the ditch height). TSS of secondary clarifier's underflow and effluent were measured weekly and once a month,

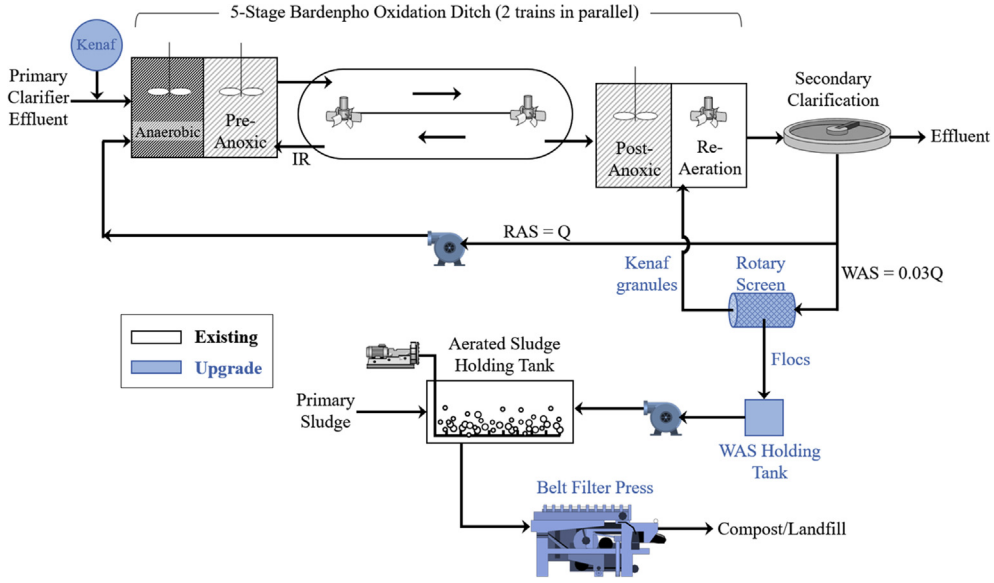

Fig. 1. Process schematic of the Town of Moorefield Advanced Nutrient WWTP.

respectively. After more than two years since the upgrade, two mixed liquor samples were collected (in May and June 2019) from the oxidation ditch and shipped overnight on ice to the University of Washington. The first sample was used for physical characteristic analyses and microscopic imaging (Section 2.3, 2.4, 2.7, 2.8) and the second sample was used for biomass-specific activity tests (Section 2.5). Morphologies of the kenaf particulates were observed at 6X-10× magnification under a Zeiss Stemi 508 stereomicroscope in dark field mode.

2.3. Wet biomass density

Density of mixed liquor sample (flocs + kenafs) and kenafs only (screened with a 212-μm sieve) were measured with a pycnometer similar to previous research (Winkler et al., 2012a). Briefly, weight of the empty pycnometer (M_{pyc}) and pycnometer filled with water (M_{pyc+w}) were first determined. Free water in the samples was removed by passing the samples through a 0.45 μm glass filter. Using a spatula, the cake (wet biomass) retained on the filter was transferred to the empty pycnometer and together the weight was measured (M_{pyc+b}). The pycnometer with the inserted biomass was then filled with water and the weight was determined ($M_{pyc+b+w}$). Density of the wet biomass was then calculated using Eq. (1):

$$\rho_b = \frac{M_b}{V_b} = \frac{M_{pyc+b} - M_{pyc}}{\frac{M_{pyc+w} - M_{pyc}}{\rho_w} - \frac{M_{pyc+b+w} - M_{pyc+b}}{\rho_w}} \quad (1)$$

where:

ρ_b = density of biomass, g $L.^{-1}$

M_b = mass of biomass, g.

V_b = volume of biomass, L.

M_{pyc+b} = mass of pycnometer containing biomass, g.

M_{pyc} = mass of pycnometer, g.

M_{pyc+w} = mass of pycnometer containing water, g.

$M_{pyc+b+w}$ = mass of pycnometer containing biomass and water, g.

ρ_w = density of water at temperature of experiment, g $L.^{-1}$

2.4. Particle size distribution

The particle size distribution of the mixed liquor sample was determined with sieve analysis. Samples were passed through a series of sieves (3-in diameter) with various mesh sizes (van Loosdrecht et al., 2016). Starting from the sieve with the largest mesh size, a sample was passed through and only particles larger than the mesh size were retained. Gentle washing with DI water was done to help push through any particles smaller than the mesh size. All water and solids passing through the sieve were captured and the procedure was repeated with all the remaining sieves in order of reducing mesh sizes. Solids captured on each sieve was then backwashed into an individual beaker per granule size fraction and the g of TSS was measured per Section 2.6. The particle size distribution was determined by g TSS of each size over the sum of g TSS of all sizes.

2.5. Specific activity tests

Specific activity tests were performed to measure the ammonia oxidation, phosphorus release, phosphorus uptake, and heterotrophic denitrification activities. All tests were conducted using separate aliquots of the same mixed liquor sample collected in June 2019. Before each activity test, the mixed liquor sample was first aerated for 1.5–2 h at room temperature. A 425-μm sieve was used to screen out the flocs in the mixed liquor to ensure only large biofilm particulates (kenaf particles) were used. The kenafs were then aerated for another 15 min in a media consisting of 44 mg L^{-1} $MgSO_4 \cdot 7H_2O$, 17.5 mg L^{-1} KCl, and 0.5 mL of Vishniac trace element solution (Vishniac and Santer, 1957). The tests were conducted in 500-mL graduated cylinders with liquid volume of 200 mL at 20 °C in biological duplicates (e.g., two individual mixed liquor aliquots were subjected to the same procedures for measuring ammonia oxidation in two separate cylinders). The g of VSS in each cylinder was determined at the end of the test. For ammonia oxidation activity, 30 mg N L^{-1} of NH_4^+ was spiked into the cylinder and NH_4^+ concentrations were monitored over time while sparged with air. 0.01 M of phosphate buffer was added to control pH at 7.39 ± 0.02. For the P release activity test, the cylinders were first sparged with

N_2 gas for about 10 min then spiked with 150 mgCOD L^{-1} of acetate. PO_4^{3-} and acetate concentrations were monitored over time while sparged with N_2 gas. Immediately after the P release test, granules were transferred into new media free of acetate for the P uptake activity test. Transferring was done with N_2-parged water to provide anaerobic starting conditions. Samples were then aerated and once the DO reached saturation, 100 mg L^{-1} PO_4^{3-}-P and 6 mg L^{-1} NH_4^+-N were spiked into the cylinders. PO_4^{3-} concentrations were monitored over time while sparged with air. For heterotrophic denitrification test, the cylinders were sparged with N_2 gas first for 10 min then spiked with 150 mgCOD L^{-1} of acetate, 30 mg L^{-1} of NO_3^--N and 6 mg L^{-1} NH_4^+-N. Concentrations of COD and NO_3^- were monitored over time while sparged with N_2 gas.

2.6. Analytical methods

Suspended and volatile solids (TSS and VSS) were analyzed according to Standard Methods 2540D and 2540 E. The SVI_5 and SVI_{30} (mL g^{-1}) were determined from the settled volume (mL) of a mixed liquor sample, after 5 and 30 min settling in a 1-L graduated cylinder, divided by g TSS. Using the Gallery™ Automated Photometric Analyzer and the Gallery™ system reagents (all by Thermo Fisher Scientific), concentrations of NH_4^+, NO_2^-+NO_3^-, NO_2^-, and PO_4^{3-} were measured according to ISO 15923−1, EPA 353.1, EPA 354.1, and EPA 365.1, respectively. Acetate concentrations were analyzed using the ion-chromatography Dionex ICS-5000 system with the IonPac® ICE-AS6 column (both by Thermo Fisher Scientific).

2.7. Determination of biomass fraction of kenaf particles

Kenaf biofilm particles (screened with a 212-μm sieve) were sparged with air for 1 h and stained with 1.5 μL of SYTO™ 9 Green Fluorescent Nucleic Acid Stain (Thermo Fisher Scientific) per mL of cellular content, then incubated in dark for 15 min. Z stacks were used to image cross sections throughout the biofilm particles. To confirm z-stack cross section, a 100 μm section was sliced from a kenaf particle using a cryostat (Thermo Scientific CryoStar NX50). Staining and microscopy were done on the section following the same protocol as the whole biofilm particles. A total of 4 z-stack images and 1 cryotome-sliced image were obtained from 2 kenaf particles. Software processing to determine biomass volume fractions was done for all 5 images using ImageJ.

2.8. Fluorescence in-situ hybridization (FISH)

Water was first removed from the mixed liquor sample by centrifugation and removal of supernatant. Then, the pellet was resuspended in 4% paraformaldehyde and let sit on ice for 120 min. The paraformaldehyde was washed off by centrifugation, removal of supernatant, and resuspension in 1x PBS. The final resuspension was in an ethanol and PBS solution at 1.25:1 volumetric ratio and stored at −20 °C. Kenaf biofilm particulates were frozen in a tissue freezing medium at −20 °C and cut into slices of 25-μm thickness using a cryostat (Thermo Scientific CryoStar NX50). Kenaf slices were adhered onto gelatin-coated microscopic glass slides. The slices were then dried at 46 °C and dehydrated with subsequent (3 min each) 50%, 80%, and 98% ethanol concentrations. For each well, 10 μL of hybridization buffer solution was added consisting of 0.9 M NaCl, 0.02 M Tris-HCl (pH 8.0), 35% formamide, and 0.02% sodium dodecyl sulfate (SDS). Subsequently, 1 μL of 5 μM probe mix was added for each well. The FISH probe mix included PAO462/PAO651/PAO846 for targeting *Candidatus* Accumulibacter (Crocetti et al., 2000) and NSO190/NSO1225 for targeting ammonia oxidizing bacteria (AOB) (Mobarry et al., 1996) (sequences are listed in Table S2). A recent study evaluated the widely used FISH probes for targeting ammonia oxidizing betaproteobacteria (*β*-AOB) and offered newly designed probes with better or similar coverage as the established probes (Lukumbuzya et al., 2020). For the *β*-AOB probes used in this study, Lukumbuzya et al. (2020) showed that NSO190 covers *β*-AOB incompletely whereas NSO1220 still offers excellent coverage. Hybridization step took place in a humid chamber at 46 °C overnight. Immediately after hybridization, the un-hybridized probes were washed off with a washing buffer (preheated to 48 °C) consisting of 20 mM Tris-HCl (pH 8), 0.08 mM NaCl, 5 mM EDTA (pH 8.0), and 0.01% SDS. Washing was performed by first rinsing with the washing buffer and then immersing the slide into the washing buffer for 20 min. After a final rinse with milliQ water and air drying at room temperature, antifade fluorescent mounting medium (20 mM Tris at pH 8.0, 0.5% N-propyl gallate, and 90% glycerol) with 0.05 μg L^{-1} of DAPI was added to each well and covered with a cover slip. Slide was observed using a confocal microscope (Zeiss Axioskop 2 MOT) fitted with a Zeiss Axiocam 503 mono camera.

3. Results and discussion

3.1. Startup and system performance

3.1.1. Improved treatment capacity

Once operations started in early March of 2017, there was a gradual decrease in mixed liquor SVI_{30} from >200 mL g^{-1} to below 50 mL g^{-1} in about 5 months (Fig. 2a), which is similar to the startup time to reach mature granulation at pilot- or full-scale AGS facilities (Pronk et al., 2015, 2017; Wagner et al., 2015). In contrast to systems using plastic carriers, which requires a screen to retain the carriers inside the aeration basin to avoid operational issues, the kenaf biofilm particles can convey freely into the secondary clarifiers to improve settling performance and lower the effluent TSS (Fig. 2c). Before the upgrade, the SRT of the Plant was 26.5 ± 6.8 days. After the MOB™ process started, the average solids concentrations of the clarifier underflow (Fig. 2b) and WAS flowrate (2.08 ML $week^{-1}$) did not vary over time, but only solids that passed

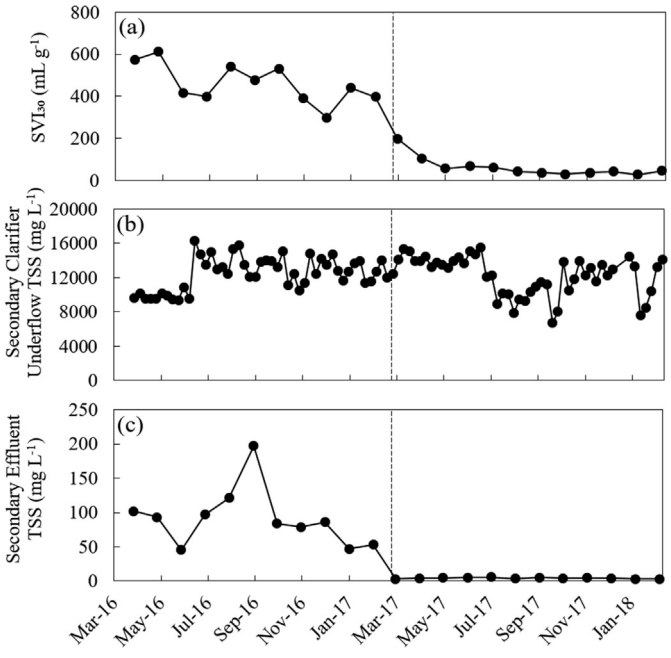

Fig. 2. (a) Monthly SVI_{30}, (b) weekly secondary clarifier underflow TSS, and (c) monthly secondary effluent TSS; dashed vertical line indicates time of upgrade.

through the rotary drum screen (flocs) were wasted and kenaf particles were retained in the system. As a result, the kenaf and flocculent SRTs were decoupled. However, how much the SRTs were decoupled was unknown because the Plant's measurements on MLSS and waste solids did not separate kenaf particles and flocs, and thus it is recommended to obtain additional measurements to reflect the separation of SRTs. After the upgrade, less solids were wasted as kenaf biofilm particles were retained, which should ultimately lead to higher MLSS concentrations. However, the Plant reported lower MLSS (4005 ± 818 mg L^{-1}) after the upgrade in comparison to before (5655 ± 576 mg L^{-1}) (Fig. S4). In SBR-type AGS systems, it is common that the MLSS at the bottom is higher than the MLSS at the top of the reactor because the larger granules are too heavy to be evenly suspended and tend to concentrate on the bottom (Pronk et al., 2014; Winkler et al., 2011b). Such phenomenon likely occurred at this plant as well and due to the sampling location being near the top (4 ft from the surface), the mixed liquor sample collected may have under-represented the actual MLSS in the oxidation ditch, emphasizing the need for better mixing, sampling, and sludge management procedures in granule type systems.

3.1.2. EBPR and nitrification capacity

There were minimal variations in influent TP loading (Fig. S2) and effluent TP concentrations (Fig. 3a) before versus after the upgrade, but there was an obvious 25% reduction in the average sodium aluminate usage from 61,000 to 46,000 kg $month^{-1}$ (Fig. S5). The amount of sodium aluminate (added at the primary clarifier) was manually adjusted depending on the biological P removal performance at the oxidation ditch (based on the effluent TP concentrations), and thus a decrease in chemical usage indicated an increase in the enhanced biological phosphors removal (EBPR) capacity. This improvement was likely due to buildup of polyphosphate-accumulating organism biomass from the increase of solids inventory that intensified the treatment capacity of existing infrastructure. In addition, biofilm systems are more tolerant to pH/temperature shocks and inhibitory substances in comparison to flocculent sludge due to shielding of microorganisms within the protective biofilm structure (Liu et al., 2015; Lourenco et al., 2015; Pronk et al., 2015). As the nitrogen loading was already below the capacity prior to the upgrade, there was no obvious changes in the nitrogen removal efficiency after the addition of kenaf carriers (Fig. 3b and c). The elevated effluent ammonia and nitrate/nitrite concentrations during the Winter months of 2017 might be due to a system upset in combination with low temperature, which led to a reduction in biofilm area specific removal rates. The performance recovered toward the start of Spring. Previous research had demonstrated that in a flocculent system with minimal nitrification capacity (low temperature and SRT), high ammonia oxidation efficiency can be achieved by bioaugmentation with granules (Figdore et al., 2018). Such system requires that granules be separated from flocs and retained in the system, which is feasible with the kenaf particles and rotary drum screen as shown in this study. Therefore, it is expected that the Plant can handle higher future nitrogen loading with the integration of mobile kenaf biofilm particles.

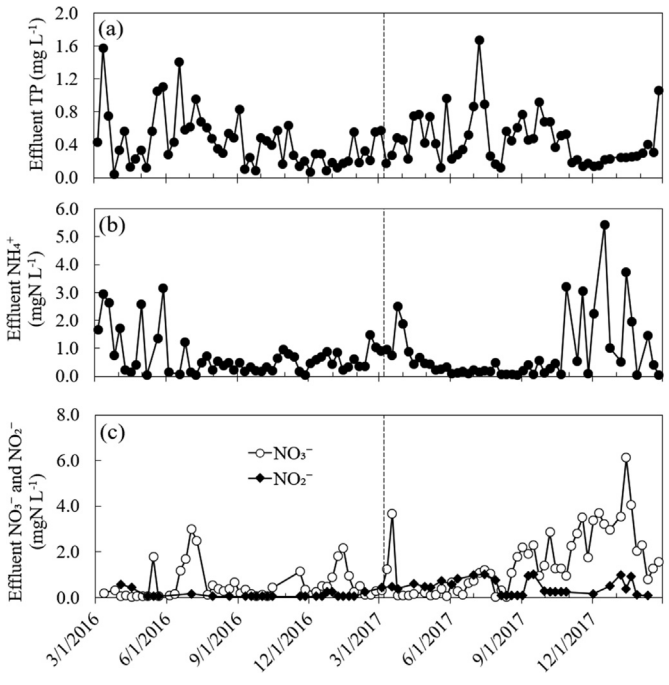

Fig. 3. Weekly average effluent (a) TP, (b) NH_4^+, and (c) NO_3^-/NO_2^- concentrations; dashed vertical line indicates time of upgrade.

3.2. Physical characteristics of kenaf biofilm particulates

After more than two years since the upgrade, the kenaf particles were collected for further examinations. The kenafs had clear development of biofilm on the surface (Fig. S3b) and the cylindric-oval structure and smooth surface indicated granular morphologies (Fig. 4). Microscopic image of a 25-μm thick biofilm section showed a fibrous interior structure covered by an outer bacterial layer with an average thickness of 75 μm (Fig. S6). The mechanisms of biofilm growth on the kenaf particles were not studied but according to literature, the key processes for biofilm development likely involved cell attachment onto the media surface, microbial adhesion enhancement by production of extracellular polymeric substances, and expansion of microcolonies and biofilm matrix (di Biase et al., 2019; Winkler et al., 2018). Particles size distribution analysis showed that the majority (60%) of the kenaf granules fell in the size range of 600–1400 μm and flocs (<212 μm) accounted for 13% of the total TSS (Fig. S7). The density of mixed liquor was 1032 ± 0.4 g L^{-1} while the density for kenaf granules alone was slightly higher at 1035 ± 0.9 g L^{-1}. These densities are on the high end in comparison to values measured for lab-scale aerobic granules cultivated in EBPR SBRs, which vary from 1004 ± 4 to 1018 ± 13 g L^{-1} for granules enriched with glycogen-accumulating organisms (GAO) and polyphosphate-accumulating organisms (PAO), respectively (Winkler et al., 2011a). The higher density of the kenaf granules may be attributed to the high specific gravity of 1.059 of the media. Kenaf granules alone exhibited similar settling characteristics to granular sludge with an SVI_{30} of 30.6 mL g^{-1} and SVI_5/SVI_{30} ratio of 1.0. Interestingly, there appears to be the presence of semi-spherical granules as opposed to the elongated morphologies of the kenaf particles (Fig. 4). It has been shown in previous research that in continuous-flow systems, there is a constant exchange of biomass between granules and flocs where they undergo dynamic processes of aggregation, attachment, and breakage (Zhou et al., 2014). Therefore, it is possible that these semi-spherical aggregates were formed by biofilm detachment from the kenaf granules.

Due to starvation and anaerobic conditions, the core of aerobic granules is usually inactive, consisting of dead cells, proteins, and inorganic precipitates (McSwain et al., 2005). The biomass fraction of the kenaf granules was determined to be 38 ± 8%. For comparison, the biomass fraction of aerobic granules collected from a pilot-scale SBR treating centrate (Armenta et al., 2019) was also measured and the value was 34 ± 5%. It is known that endogenous

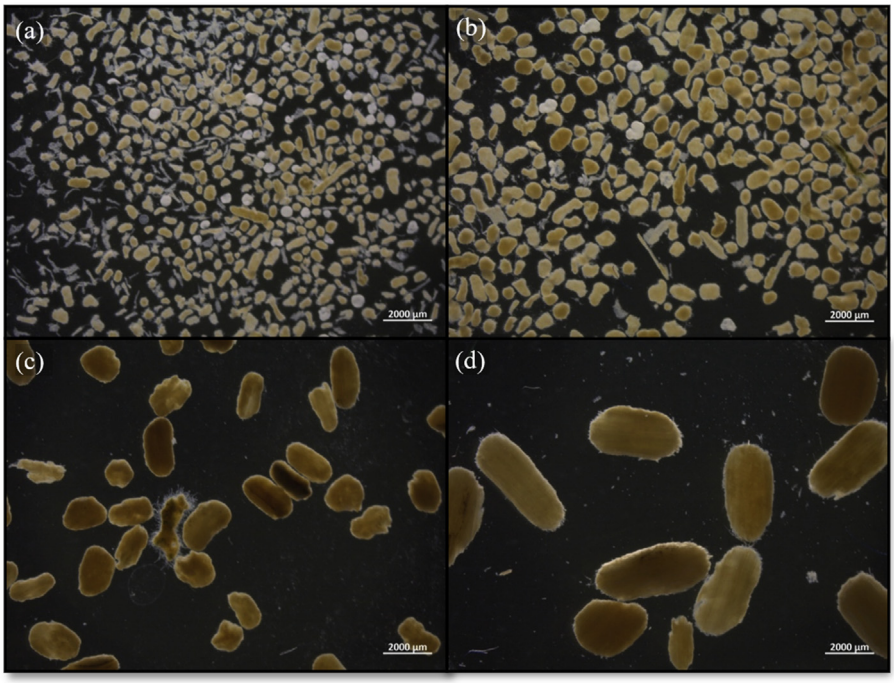

Fig. 4. Stereomicroscopic images of kenaf granules of size ranges (a) 212–425 µm, (b) 425–600 µm, (c) 850–1180 µm, and (d) 1700–2000 µm taken in darkfield mode at 6.3X.

decay occurs in the core of aerobic granules due to substrate diffusion limitations, and thus as granule size increases the inner structure of the granules will weaken and granule breakage will occur (Verawaty et al., 2013; Winkler et al., 2012b). Breakage of the kenaf granules was not studied. However, the core of kenaf granules consists of lignocellulose material, which is non-degradable for most of the common microorganisms found in activated sludge (de Souza, 2013). Therefore, it is possible that the kenaf core offers a stronger backbone to withstand hydrolysis and breakage in comparison to aerobic granules, allowing for better tolerance to pumping or shearing in the rotary drum screen.

3.3. Specific activity of key functional groups

The specific activity of the kenaf granules are presented in Table 1 in comparison with values reported in the literature for full-scale SBR-type AGS plants. The specific ammonia uptake rate (SNUR) was 50% lower than the Nereda® SBR, and a possible explanation is the high influent C/N ratio of Moorefield WWTP. Lower influent C/N ratio is known to enrich for nitrifiers due to less competition with heterotrophs for substrates and space (Bassin et al., 2012; Satoh et al., 2000). The influent BOD/TN ratio was 20 for Moorefield WWTP whereas the Nereda® SBR plant (Pronk et al., 2015) had a ratio of 4.2. The higher BOD/TN ratio of this study indicated that per unit of biomass, more heterotrophs would compete for the nitrogen and less nitrogen was available for nitrifier growth, which may explain the lower SNUR of this study. The specific phosphorus uptake rate (SPUR) of the kenaf granules was similar to or higher than the aerobic granules.

The FISH images showed clusters of AOBs and PAOs randomly mixed throughout the outer 50–60 µm layer of the kenaf granules (Fig. 5). In SBR-type AGS systems with no anoxic phase, denitrification must occur during the aerobic phase within the anoxic layer of the granules. This is enabled by the stratified microbial

Table 1
Specific activity values of kenaf granules in comparison with values reported at full-scale aerobic granular sludge SBR plants.

		Kenaf granules	Aerobic granules	
	Process	Continuous flow	Nereda® SBR	SBR
	Influent	90% poultry; 10% domestic	100% domestic	30–40% dairy; 60–70% domestic
	Reference	This study	Pronk et al. (2015)	Świątczak and Cydzik-Kwiatkowska (2018)
Parameter[a]	Unit		Values[b]	
DO	mg L^{-1}	>8.6[c]	1.8–2.5	<2.0
Temp.	°C	20	20	N/A
SNUR	mg NH_4^+-N (gVSS d)$^{-1}$	13.9 ± 0.3	28[d]	6.1
SPRR	mg PO_4^{3-}-P (gVSS d)$^{-1}$	95.3 ± 0.8	N/A	N/A
SPUR	mg PO_4^{3-}-P (gVSS d)$^{-1}$	38.2 ± 0.8	40[d]	17.2
SDNR	mg NO_3^--N (gVSS d)$^{-1}$	32.2 ± 4.7[e]	N/A	N/A

[a] SNUR = specific ammonia-N uptake rate; SPRR = specific P release rate; SPUR = specific P uptake rate; SDNR = specific heterotrophic denitrification rate.
[b] Values for AGS SBRs were estimated from the reported volumetric conversion rates measured directly from a reactor cycle.
[c] Acitivty tests were conducted at saturation DO. The process DO of the Plant was 0.35–0.5 mg L^{-1}.
[d] 8000 mg L^{-1} MLSS and 25% ash content were used for the calculation based on available information in the paper.
[e] The acetate used per NO_3^- denitrified was 16.6 ± 2.4 gCOD gN^{-1}.

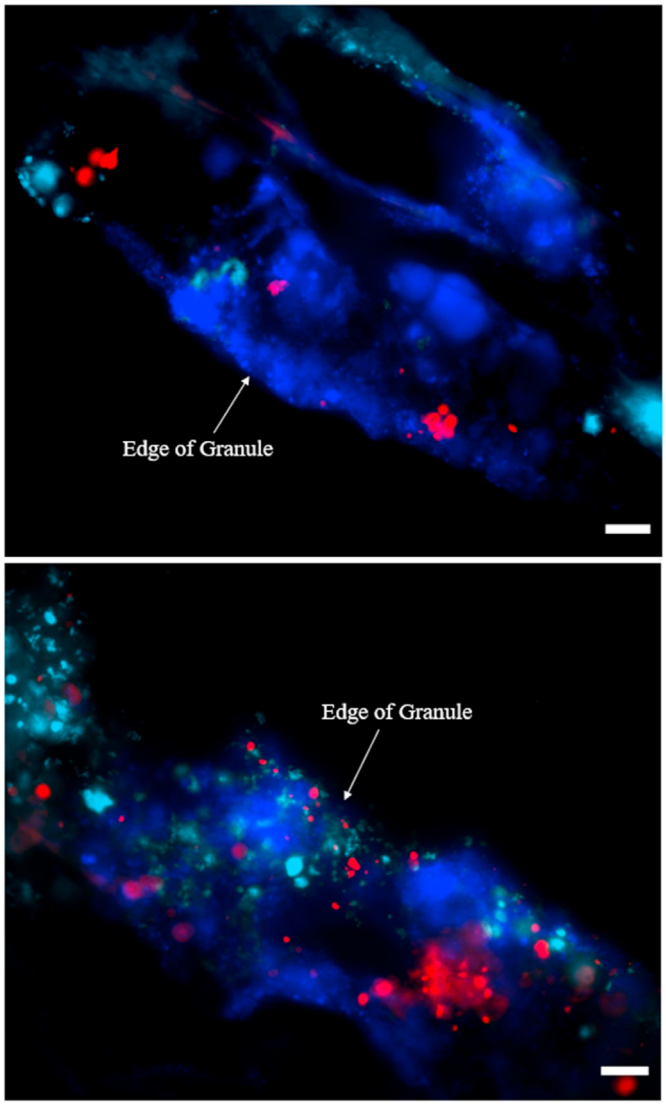

Fig. 5. FISH images of 25 μm-thick kenaf granule sections; Cy5 (cyan) = PAO, Cy3 (red) = AOB, and DAPI (blue) = all bacteria. Scale bar = 20 μm. (For interpretation of the references to colour in this figure legend, the reader is referred to the Web version of this article.)

distribution where nitrifiers typically inhabit the outer oxygen-penetrated shell to oxidize NH_4^+ into NO_2^-/NO_3^-, which are then used as electron acceptors for denitrification by denitrifying PAOs (dPAO) in the anoxic inner layers, as typically observed in SBR-type AGS systems fed with VFAs (de Kreuk et al., 2005; Winkler et al., 2013). In this study the application of kenaf granules were in a continuous flow system with separated anaerobic, anoxic, and aerobic zones, thus the need for high simultaneous nitrification-denitrification (SND) efficiency in a single reactor and a stratified AOB/PAO distribution in a single granule was not necessary for meeting overall TN removal requirements. Therefore, the lack of stratified distribution of AOB/PAO observed in the kenaf granules (Fig. 5) was expected.

This lack of stratified distribution in continuous flow systems can be explained by several factors: (1) usage of recycled nitrate by dPAO that can occur throughout the granule depth in the anoxic zone, hence eliminating the need for dPAO growth in deeper granule layers, (2) consumption of PAO's intracellular carbon storage occurred partially in the anoxic zone, leaving less carbon availability for denitrification in the subsequent aerobic zone and thus less dPAO growth in the anoxic layer, and (3) utilization of intracellular carbon and slowly biodegradable carbon by PAO and ordinary denitrifiers, respectively, using nitrate in the anoxic zone, leading to less O_2 consumption by the heterotrophs in the aerobic phase and thus higher oxygen diffusion into the granules for AOBs growth in deeper layer. On the other hand, in SBR-type AGS systems without anoxic phase, PAOs and ordinary heterotrophs consume the carbon using oxygen in the aerobic phase, leading to less oxygen diffusion into the granule and thus less oxygen availability for growth of AOBs that share the outer-most layer with heterotrophs. In addition, it must be noted that AGS reactors treating real municipal wastewater have been shown to have much lower SND efficiencies (14–39%) compared to VFA-fed reactors (90%) and the availability of anoxic condition is highly dynamic and dependable upon the composition of wastewater and size of granules (Layer et al., 2020). Therefore, the assumption that a stratified distribution of microbial functional groups exists along the granule depth may not be as distinct in full-scale systems and requires further research.

4. Conclusions

Aerobic granular sludge is a promising technology for process intensification and its integration into continuous flow activated sludge systems is the next challenge. In this study, an appealing technology is presented that accomplished this concept with all organic mobile kenaf biocarriers, which were added to a full-scale continuous flow facility. Kenaf particles were retained in the system with a rotary drum screen fitted after the secondary clarifier underflow while flocs were selectively wasted. Biofilm developed on the kenaf media, leading to the formation of organic particles that have the same visual appearance as aerobic granular sludge. Kenaf granules had comparable settling characteristics and biomass-specific ammonia oxidation and phosphorus removal activities as aerobic granules. Furthermore, integration of the kenaf biofilm process led to lower effluent TSS concentrations and improved EBPR capacity. It is recommended that better sludge management procedures be taken for integrated continuous flow granular sludge systems as the real solids concentrations may be significantly underestimated with the traditional MLSS measurement techniques for activated sludge. Another key benefit of these all organic biofilm aggregates is that they may not need to be landfilled as the case for other plastic carriers. This is the first full-scale application of all organic and mobile biofilm technology in continuous-flow system.

Author contribution

Stephany Wei: Writing – original draft preparation, Writing-Review & Editing, Investigation, Visualization. Bao Nguyen Quoc: Investigation, Visualization. Madelyn Shapiro: Investigation. Pin Hsuan Chang: Investigation, Visualization. Jason Calhoun: Conceptualization, Methodology. Mari Winkler: Writing- Review & Editing, Supervision.

Declaration of competing interest

The authors declare that they have no known competing financial interests or personal relationships that could have appeared to influence the work reported in this paper.

Acknowledgements

This work was supported by the University of Washington

startup grant. We thank Dr. Reinhard Hübner for connecting UW with Nuvoda, making this collaboration possible, and Dr. Joshua Boltz for his comments on this manuscript.

Appendix A. Supplementary data

Supplementary data to this article can be found online at https://doi.org/10.1016/j.chemosphere.2020.129522.

References

Akil, H.M., Omar, M.F., Mazuki, A.A.M., Safiee, S., Ishak, Z.A.M., Abu Bakar, A., 2011. Kenaf fiber reinforced composites: a review. Mater. Des. 32 (8–9), 4107–4121.

Armenta, M., Stensel, H.D., Bucher, B., Sukapanpotharam, P., Nguyen Quoc, B., Winkler, M.K.H., 2019. Operation and performance of sidestream aerobic granular sludge nitrifying reactor. In: WEF Nutrient Removal and Recovery Symposium WEF Nutrient Removal and Recovery Symposium. Minneapolis, MN.

Bassin, J.P., Kleerebezem, R., Rosado, A.S., van Loosdrecht, M.C.M., Dezotti, M., 2012. Effect of different operational conditions on biofilm development, nitrification, and nitrifying microbial population in moving-bed biofilm reactors. Environ. Sci. Technol. 46 (3), 1546–1555.

Crocetti, G.R., Hugenholtz, P., Bond, P.L., Schuler, A., Keller, J., Jenkins, D., Blackall, L.L., 2000. Identification of polyphosphate-accumulating organisms and design of 16S rRNA-directed probes for their detection and quantitation. Appl. Environ. Microbiol. 66 (3), 1175–1182.

de Kreuk, M., Heijnen, J.J., van Loosdrecht, M.C.M., 2005. Simultaneous COD, nitrogen, and phosphate removal by aerobic granular sludge. Biotechnol. Bioeng. 90 (6), 761–769.

de Souza, W.R., 2013. Microbial degradation of lignocellulosic biomass. In: Chandel, A.K., Silva, S.S. (Eds.), Sustainable Degradation of Lignocellulosic Biomass - Techniques, Applications and Commercialization.

di Biase, A., Kowalski, M.S., Devlin, T.R., Oleszkiewicz, J.A., 2019. Moving bed biofilm reactor technology in municipal wastewater treatment: a review. J. Environ. Manag. 247, 849–866.

Figdore, B.A., Stensel, H.D., Winkler, M.K.H., 2018. Bioaugmentation of sidestream nitrifying-denitrifying phosphorus-accumulating granules in a low-SRT activated sludge system at low temperature. Water Res. 135, 241–250.

Kent, T.R., Bott, C.B., Wang, Z.W., 2018. State of the art of aerobic granulation in continuous flow bioreactors. Biotechnol. Adv. 36 (4), 1139–1166.

Layer, M., Villodres, M.G., Hernandez, A., Reynaert, E., Morgenroth, E., Derlon, N., 2020. Limited simultaneous nitrification-denitrification (SND) in aerobic granular sludge systems treating municipal wastewater: mechanisms and practical implications. Water Res. X 7.

Li, A.J., Li, X.Y., Yu, H.Q., 2011. Granular activated carbon for aerobic sludge granulation in a bioreactor with a low-strength wastewater influent. Separ. Purif. Technol. 80 (2), 276–283.

Liu, Y.Q., Lan, G.H., Zeng, P., 2015. Resistance and resilience of nitrifying bacteria in aerobic granules to pH shock. Lett. Appl. Microbiol. 61 (1), 91–97.

Lourenco, N.D., Franca, R.D.G., Moreira, M.A., Gil, F.N., Viegas, C.A., Pinheiro, H.M., 2015. Comparing aerobic granular sludge and flocculent sequencing batch reactor technologies for textile wastewater treatment. Biochem. Eng. J. 104, 57–63.

Lukumbuzya, M., Kristensen, J.M., Kitzinger, K., Pommerening-Röser, A., Nielsen, P.H., Wagner, M., Daims, H., Pjevac, P., 2020. A refined set of rRNA-targeted oligonucleotide probes for in situ detection and quantification of ammonia-oxidizing bacteria. Water Res. 186, 116372.

McSwain, B.S., Irvine, R.L., Hausner, M., Wilderer, P.A., 2005. Composition and distribution of extracellular polymeric substances in aerobic flocs and granular sludge. Appl. Environ. Microbiol. 71 (2), 1051–1057.

Mobarry, B.K., Wagner, M., Urbain, V., Rittmann, B.E., Stahl, D.A., 1996. Phylogenetic probes for analyzing abundance and spatial organization of nitrifying bacteria. Appl. Environ. Microbiol. 62 (6), 2156–2162.

Pijuan, M., Werner, U., Yuan, Z.G., 2011. Reducing the startup time of aerobic granular sludge reactors through seeding floccular sludge with crushed aerobic granules. Water Res. 45 (16), 5075–5083.

Pronk, M., Bassin, J.P., de Kreuk, M.K., Kleerebezem, R., van Loosdrecht, M.C.M., 2014. Evaluating the main and side effects of high salinity on aerobic granular sludge. Appl. Microbiol. Biotechnol. 98 (3), 1339–1348.

Pronk, M., de Kreuk, M.K., de Bruin, B., Kamminga, P., Kleerebezem, R., van Loosdrecht, M.C.M., 2015. Full scale performance of the aerobic granular sludge process for sewage treatment. Water Res. 84, 207–217.

Pronk, M., Giesen, A., Thompson, A., Robertson, S., van Loosdrecht, M., 2017. Aerobic granular biomass technology: advancements in design, applications and further developments. Water Pract. Technol. 12 (4), 987–996.

Ramesh, M., 2016. Kenaf (Hibiscus cannabinus L.) fibre based bio-materials: a review on processing and properties. Prog. Mater. Sci. 78–79, 1–92.

Satoh, H., Okabe, S., Norimatsu, N., Watanabe, Y., 2000. Significance of substrate C/N ratio on structure and activity of nitrifying biofilms determined by in situ hybridization and the use of microelectrodes. Water Sci. Technol. 41 (4–5), 317–321.

Sturm, B., Faraj, R., Figdore, B., Willoughby, A., Ford, A., Bott, C., Shiskowski, D., McFall, L., Downing, L., 2017. Balancing Granular Sludge with Activated Sludge Systems for Biological Nutrient Removal. WEFTEC Conference Proceedings, Chicago, IL.

Świątczak, P., Cydzik-Kwiatkowska, A., 2018. Performance and microbial characteristics of biomass in a full-scale aerobic granular sludge wastewater treatment plant. Environ. Sci. Pollut. Res. 25 (2), 1655–1669.

van Loosdrecht, M.C., Nielsen, P.H., Lopez-Vazquez, C.M., Brdjanovic, D., 2016. Experimental methods in wastewater treatment. Water Intell. Online 15, 9781780404752.

Verawaty, M., Tait, S., Pijuan, M., Yuan, Z.G., Bond, P.L., 2013. Breakage and growth towards a stable aerobic granule size during the treatment of wastewater. Water Res. 47 (14), 5338–5349.

Vishniac, W., Santer, M., 1957. The thiobacilli. Bacteriol. Rev. 21 (3), 195.

Wagner, J., Guimaraes, L.B., Akaboci, T.R.V., Costa, R.H.R., 2015. Aerobic granular sludge technology and nitrogen removal for domestic wastewater treatment. Water Sci. Technol. 71 (7), 1040–1046.

Winkler, M.-K., Bassin, J., Kleerebezem, R., De Bruin, L., Van den Brand, T., Van Loosdrecht, M., 2011a. Selective sludge removal in a segregated aerobic granular biomass system as a strategy to control PAO–GAO competition at high temperatures. Water Res. 45 (11), 3291–3299.

Winkler, M.K.H., Bassin, J.P., Kleerebezem, R., de Bruin, L.M.M., van den Brand, T.P.H., van Loosdrecht, M.C.M., 2011b. Selective sludge removal in a segregated aerobic granular biomass system as a strategy to control PAO-GAO competition at high temperatures. Water Res. 45 (11), 3291–3299.

Winkler, M.K.H., Bassin, J.P., Kleerebezem, R., van der Lans, R., van Loosdrecht, M.C.M., 2012a. Temperature and salt effects on settling velocity in granular sludge technology (vol 46, pg 3897, 2012). Water Res. 46 (16), 5445–5451.

Winkler, M.K.H., Kleerebezem, R., Khunjar, W.O., de Bruin, B., van Loosdrecht, M.C.M., 2012b. Evaluating the solid retention time of bacteria in flocculent and granular sludge. Water Res. 46 (16), 4973–4980.

Winkler, M.K.H., Kleerebezem, R., Strous, M., Chandran, K., van Loosdrecht, M.C.M., 2013. Factors influencing the density of aerobic granular sludge. Appl. Microbiol. Biotechnol. 97 (16), 7459–7468.

Winkler, M.K.H., Meunier, C., Henriet, O., Mahillon, J., Suarez-Ojeda, M.E., Del Moro, G., De Sanctis, M., Di Iaconi, C., Weissbrodt, D.G., 2018. An integrative review of granular sludge for the biological removal of nutrients and recalcitrant organic matter from wastewater. Chem. Eng. J. 336, 489–502.

Winkler, M.K.H., Straka, L., 2019. New directions in biological nitrogen removal and recovery from wastewater. Curr. Opin. Biotechnol. 57, 50–55.

Zhou, D.D., Niu, S., Xiong, Y.J., Yang, Y., Dong, S.S., 2014. Microbial selection pressure is not a prerequisite for granulation: dynamic granulation and microbial community study in a complete mixing bioreactor. Bioresour. Technol. 161, 102–108.